

# Full-potential spin-polarized relativistic Korringa-Kohn-Rostoker method implemented and applied to bcc Fe, fcc Co, and fcc Ni

T. Huhne, C. Zecha, and H. Ebert

*Institut für Physikalische Chemie, Universität München, Theresienstraße 37, D-80333 München, Germany*

P. H. Dederichs and R. Zeller

*Institut für Festkörperforschung, FZ Jülich, D-80333 Jülich, Germany*

(Received 24 June 1998)

The full-potential spin-polarized relativistic Korringa-Kohn-Rostoker (FP-SPR-KKR) method of band-structure calculation has been implemented in a self-consistent way. This scheme deals with the nonspherical potential as well as spin polarization and all relativistic effects on the same level. Technical details of this approach as well as its formal extension to account for the so-called orbital polarization (OP) mechanism are described in some detail. Results of corresponding applications to the elemental ferromagnets bcc-Fe, fcc-Co, and fcc-Ni are presented with an emphasis on the consequences of nonspherical and OP-potential terms.

[S0163-1829(98)05540-4]

## I. INTRODUCTION

The KKR method of band-structure calculation has been introduced already in the 1940s by Korringa<sup>1</sup> and Kohn and Rostoker.<sup>2</sup> While this scheme was not very popular in its original form it became extremely important in connection with multiple-scattering theory as a way to get access to the electronic Green's function (KKR-GF). This development opened the way to deal with solids with reduced symmetry such as, for example, impurities in an otherwise ordered host material. Another important application is the investigation of randomly disordered alloys by adding some adequate alloy theory as for example the coherent potential approximation (KKR-CPA).

Originally the KKR as well as its extensions mentioned above have been formulated on the basis of the so-called muffin-tin construction for the charge and potential distribution. First steps towards a full-potential (FP) scheme were undertaken by Anthony and Bross by using a warped muffin-tin potential.<sup>3</sup> However, the extension of the KKR to a true FP-scheme by a corresponding proper treatment of the non-constant interstitial potential between the muffin tins has been discussed in the literature for a rather long time and in a very controversial way. Now, it is generally accepted that the scheme proposed among others by Zeller and Dederichs supplies a sound basis for FP-KKR band structure calculations. In practice, this scheme essentially consists in using a Wigner-Seitz partitioning of the space and using within the corresponding atomic cells for all relevant quantities a representation in terms of spherical harmonics; i.e., for the wave functions, the Green's function as well as for the charge and potential distribution. Since its first implementation by Dritler *et al.*<sup>4</sup> the FP-KKR has been applied with great success mostly to impurity systems.<sup>5-8</sup> While this work was done in a nonrelativistic or scalar relativistic way the extension to the relativistic case has been investigated by Tamura,<sup>9</sup> Wang *et al.*,<sup>10</sup> and Lovatt, Gyorffy, and Guo.<sup>11</sup> The corresponding construction of the Green's function for the most general case that the potential entering the Dirac equation is not only

nonspherical but also spin dependent and includes a vector potential contribution has been studied in great detail by Tamura.<sup>9</sup>

Practical applications, however, have been restricted until now to the spin-polarized relativistic (SPR) case leading to the FP-SPR-KKR that has been implemented so far only in a non-self-consistent mode.<sup>11</sup> On the other hand, self-consistent calculations have been performed recently for the paramagnetic case (R-KKR) using the KKR-method in its variational form.<sup>12</sup> In addition it is worth to mention here also the use of the FP-SPR-KKR scheme within the one-step model of photoemission theory by Fluchtmann *et al.*<sup>13</sup> Similar work has been done also by Krewer and Feder<sup>14</sup> in the case of spin-polarized LEED.

In the following, we report on a self-consistent implementation of the FP-SPR-KKR Green's-function method. This includes an extension of the scheme to account for the spin-orbit-induced orbital polarization (OP) due to Brooks' OP mechanism<sup>15,16</sup> (FP-OP-SPR-KKR or FP-SOPR-KKR). In the next section, the technical details of an implementation of the FP-(OP-)-SPR-KKR scheme will be presented. This is followed by a presentation and discussion of results that have been obtained for the elemental ferromagnets bcc Fe, fcc Co, and fcc Ni as a test case.

## II. THEORETICAL FRAMEWORK AND TECHNICAL DETAILS

### A. Kohn-Sham-Dirac equation

The investigations to be presented below have been performed within the framework of the relativistic version of spin-density-functional theory (SDFT). The corresponding Dirac equation for the four-component single-particle wave function  $\Phi$  and energy  $E$ :

$$\left( \frac{c}{i} \vec{\alpha} \vec{\nabla} + \frac{1}{2} (1 - \beta) c^2 + V(\vec{r}) \right) \Phi_i(\vec{r}) = E \Phi_i(\vec{r}) \quad (1)$$

has been introduced by MacDonald and Vosko<sup>17</sup> and Rajagopal<sup>18</sup> (atomic Rydberg units used throughout; i.e.,  $\hbar = 1, m = 1/2, e^2 = 2$ ). In this Kohn-Sham-Dirac equation, the potential  $V$ ,

$$V = V_n + V_H + \bar{V}_{xc} + \beta \vec{\sigma} \vec{B}, \quad (2)$$

contains the Coulomb potential due to the nuclei ( $V_n$ ) and the other electrons ( $V_H$ ). The contribution due to exchange and correlation has been split into a spin-averaged part ( $\bar{V}_{xc}$ ) and a spin-dependent part ( $\beta \vec{\sigma} \vec{B}$ ). The effective magnetic field  $\vec{B}$  occurring in the latter term stems from the dependence of the exchange-correlation energy  $E_{xc}$  on the spin magnetization density  $\vec{m}$ :

$$\vec{B}_{eff}(\vec{r}) = \vec{B}_{ext}(\vec{r}) + \frac{\partial E_{xc}[n, \vec{m}]}{\partial \vec{m}(\vec{r})} \quad (3)$$

with  $n$  the particle density. In the calculations presented below the local exchange-correlation potential of Moruzzi, Janak, and Williams has been used.<sup>19</sup> A possible contribution from an external magnetic field  $\vec{B}_{ext}$  has been added in Eq. (II A). Finally, the quantities  $\alpha_i$  ( $i = 1, \dots, 3$ ) and  $\beta$  occurring in Eqs. (1) and (2) are the standard  $4 \times 4$  Dirac matrices and the  $\sigma_i$  ( $i = 1, \dots, 3$ ) are the Pauli spin matrices in their relativistic form.<sup>20</sup>

The spin-dependent term in Eq. (2) strongly reduces the symmetry for the above Dirac equation.<sup>21</sup> One of the many consequences of this is that inclusion of spin-orbit coupling leads for a spin-polarized system to a finite orbital magnetic moment. However, compared to experiment this is often found to be up to approximately 50% too small.<sup>22</sup> To cure this problem Brooks<sup>15,23</sup> has proposed a so-called orbital polarization (OP) term that is meant to account for Hund's second rule. Originally, this heuristic term has been added to the Hamiltonian matrix of a conventional band-structure scheme that works on a nonrelativistic or scalar relativistic level with the spin-orbit coupling treated as a perturbation in the variational step. Recently, Ebert and Battocletti<sup>16</sup> derived a corresponding potential term that can be added to the above Dirac equation. For  $d$ -electron systems it is given by

$$\mathcal{H}_{OP} = -B_{m_s}^{OP}(r) \langle \hat{l}_z \rangle_{m_s} \hat{l}_z \delta_{l2}. \quad (4)$$

Here  $\langle \hat{l}_z \rangle_{m_s}$  is the expectation value of the orbital angular momentum operator for the spin subsystem with character  $m_s$  and

$$B_{m_s}^{OP}(r) = \frac{2}{441} \int_0^r dr' 4\pi r'^2 \left( 9 \frac{r_{<}^2}{r_{>}^3} - 5 \frac{r_{<}^4}{r_{>}^5} \right) \rho_{dm_s}(r') \quad (5)$$

stems from a Racah parameter.<sup>15,23</sup> In Eq. (5)  $\rho_{dm_s}$  is the averaged charge density for a  $d$  electron and  $r_{<}$  ( $r_{>}$ ) stands for the smaller (larger) of  $r$  and  $r'$ . Obviously  $\mathcal{H}_{OP}$  can be cast into the form

$$\mathcal{H}_{OP} = -A^{OP} p_\phi, \quad (6)$$

where  $p_\phi$  is the azimuthal component of the momentum operator and  $A^{OP} = r \sin \theta B_{m_s}^{OP} \langle \hat{l}_z \rangle_{m_s} \delta_{l2}$  is a rotationally symmet-

ric vector potential normalized according to Eq. (6) and the use of atomic units. Formally the OP term has therefore a form to be expected from current-density-functional theory<sup>24,25</sup> (CDFT), which should provide a sound and rigorous basis for investigating any properties connected with orbital magnetism.<sup>26</sup> However, one has to note that the physical justification for Brooks' OP term is quite different from the exchange-correlation vector potential occurring within CDFT.<sup>27</sup>

## B. Solution of the single-site problem

To deal with the above Dirac equation for the case of a nonspherical potential we have adopted the scheme developed by Zeller and Dederichs<sup>4,6-8</sup> during recent years for the nonrelativistic or scalar relativistic case. This implies that in a first step space is subdivided into nonoverlapping, space-filling polyhedra usually realized by means of the Wigner-Seitz construction. The shape of these Wigner-Seitz cells is represented by the so-called shape functions  $\theta_L(r)$  with

$$\Theta_{WS}(\vec{r}) = \sum_L \theta_L(r) \mathcal{Y}_L(\hat{r}), \quad (7)$$

where the step function  $\Theta_{WS}$  is 1 for  $\vec{r}$  within the cell and 0 otherwise. The functions  $\mathcal{Y}_L$  are real spherical harmonics with  $L$  standing for  $(l, m)$ . In addition one defines the radius  $r_{cr}$  of the smallest circumscribed sphere, for which  $\Theta_{WS}(\vec{r}) = 0$  for  $r > r_{cr}$ . Multiplying the potential  $V$  of the extended system in Eq. (1) with the function  $\Theta_{WS}(\vec{r})$  centered at an atomic site  $n$  leading to the single-site problem. To solve the corresponding single-site Dirac equation the ansatz

$$\Phi(\vec{r}, E) = \sum_\Lambda \begin{pmatrix} g_\Lambda(r, E) \chi_\Lambda(\hat{r}) \\ if_\Lambda(r, E) \chi_{\bar{\Lambda}}(\hat{r}) \end{pmatrix} \quad (8)$$

is made. Here  $g$  and  $f$  are the radial wave functions of the major and minor components. The functions  $\chi_\Lambda$  are the conventional spin-angular functions:<sup>20</sup>

$$\chi_\Lambda = \sum_{m_s} C_\Lambda^{m_s} Y_l^{\mu - m_s} \chi_{m_s}, \quad (9)$$

with  $C_\Lambda^{m_s} = C(l, \frac{1}{2}, j; \mu - m_s, m_s)$  the Clebsch-Gordon coefficients,  $Y_l^m$  complex spherical harmonics and  $\chi_{m_s}$  the two-component Pauli spin functions.<sup>20</sup> The spin-orbit and relativistic quantum numbers,  $\kappa$  and  $\mu$ , respectively, have been combined to  $\Lambda = (\kappa, \mu)$ , with  $\bar{\Lambda} = (-\kappa, \mu)$ . Inserting  $\Phi$  into the single-site Dirac equation leads to a set of coupled radial Dirac equations:

$$\begin{aligned} \frac{\partial}{\partial r} P_\Lambda &= -\frac{\kappa}{r} P_\Lambda + \left[ \frac{E}{c^2} + 1 \right] Q_\Lambda - \frac{1}{c^2} \sum_{\Lambda'} V_{\Lambda\Lambda'}^- Q_{\Lambda'} \\ &\quad - \frac{1}{c^2} \sum_{\Lambda'} A_{\Lambda\Lambda'}^{OP} Q_{\Lambda'}, \end{aligned} \quad (10)$$

$$\frac{\partial}{\partial r} Q_\Lambda = \frac{\kappa}{r} Q_\Lambda - E P_\Lambda + \sum_{\Lambda'} V_{\Lambda\Lambda'}^+ P_{\Lambda'} + \sum_{\Lambda'} A_{\Lambda\Lambda'}^{OP} P_{\Lambda'}. \quad (11)$$

Here the arguments  $r$  and  $E$  have been suppressed for the radial wave functions for which we used the auxiliary functions

$$P_{\Lambda}(r, E) = r g_{\Lambda}(r, E), \quad (12)$$

$$Q_{\Lambda}(r, E) = c r f_{\Lambda}(r, E). \quad (13)$$

The potential matrix elements  $V_{\Lambda\Lambda'}^{\pm}$  are defined by

$$V_{\Lambda\Lambda'}^{\pm}(r) = \langle \chi_{\pm\Lambda} | V_{eff}^{\pm} \vec{\sigma} \vec{B} | \chi_{\pm\Lambda'} \rangle. \quad (14)$$

These are straightforwardly evaluated by expanding the potential into real spherical harmonics:

$$V(\vec{r}) = \sum_L V_L(r) \mathcal{Y}_L(\hat{r}), \quad (15)$$

$$B(\vec{r}) = \sum_L B_L(r) \mathcal{Y}_L(\hat{r}), \quad \text{with } \vec{B}(\vec{r}) = B(\vec{r}) \hat{B}. \quad (16)$$

Here it has been assumed that  $\vec{B}$  points everywhere along the same direction  $\hat{B}$ . In the following applications  $\hat{B}$  will be oriented along the crystallographic  $z$  axis of a bcc or fcc system. However, these are not necessary restrictions for the formalism; i.e., treatment of other orientations or noncollinear magnetic states can be straightforwardly accounted for. Finally, the potential matrix elements  $A_{\Lambda\Lambda'}^{OP}(r)$  are connected to the operator  $\mathcal{H}_{OP}$  in Eq. (6) and are defined analogously to  $V_{\Lambda\Lambda'}^{\pm}(r)$  in Eq. (14).

Restricting the above expansion for the potential  $V$  to  $L = (0,0)$  and setting  $B=0$  obviously leads to the standard radial Dirac equation for a spherical potential.<sup>20</sup> Allowing  $V$  to have nonspherical contributions with  $B=0$  one has the paramagnetic case investigated recently by Bei der Kellen and Freeman.<sup>12</sup> Retaining for  $V$  and  $B$  only the term  $L = (0,0)$  leads to the equations for spin-polarized systems derived by Doniach and Sommers,<sup>28</sup> Feder, Rosicky, and Ackermann<sup>29</sup> and Strange, Staunton, and Gyorffy<sup>30</sup> that have been used routinely for several years. For this case the  $(0,0)$  term of  $B$  already leads to a coupling of an infinite number of partial waves ( $P_{\Lambda}, Q_{\Lambda}$ ) for the same quantum number  $\mu$ . Fortunately it is well justified to restrict the coupling to  $\Delta l = l - l' = 0$ .<sup>31</sup> Inclusion of nonspherical terms in  $V$  and  $B$  lead to further coupling. In practice, however, the number of coupled partial waves is restricted to  $2(l_{max} + 1)^2$  by fixing an upper limit  $l_{max}$  for the angular momentum expansion of the wave function in Eq. (8). For example, for  $l_{max} = 2$  one may have up to 18 partial waves coupled; i.e., one has to solve up to 36 coupled equations for the functions  $P_{\Lambda}$  and  $Q_{\Lambda}$ . However, for a cubic system with  $\hat{B} = \hat{z}$  and  $l_{max} = 2$  one has at most 3 partial waves coupled due to the high symmetry of the system.

Using the above radial differential equations a set of  $2(l_{max} + 1)^2$  linearly independent regular solutions  $\Phi_{\Lambda}$  can be created by initializing the outward integration with a selected spin-angular character  $\Lambda$  dominating close to the nucleus; i.e., one demands that

$$\Phi_{\Lambda}(\vec{r}, E) = \sum_{\Lambda'} \Phi_{\Lambda'\Lambda}(\vec{r}, E) \xrightarrow{r \rightarrow 0} \Phi_{\Lambda\Lambda}(\vec{r}, E). \quad (17)$$

After having solved all systems of coupled equations for the wave functions  $\Phi_{\Lambda}$  one gets the corresponding single-site  $t$  matrix by introducing the auxiliary matrices  $a$  and  $b$ :

$$a_{\Lambda\Lambda'}(E) = -i p r^2 [h_{\Lambda}^{-}(p\vec{r}), \Phi_{\Lambda\Lambda'}(\vec{r}, E)]|_{r=r_{cr}}, \quad (18)$$

$$b_{\Lambda\Lambda'}(E) = i p r^2 [h_{\Lambda}^{+}(p\vec{r}), \Phi_{\Lambda\Lambda'}(\vec{r}, E)]|_{r=r_{cr}}. \quad (19)$$

Here  $p = \sqrt{E(1 + E/c^2)}$  is the relativistic momentum<sup>20</sup> and  $[\dots]_r$  denotes the relativistic form of the Wronskian.<sup>32</sup> The functions  $h_{\Lambda}^{\pm}$  are the relativistic version of the Hankel functions of the first and second kind:<sup>20</sup>

$$h_{\Lambda}^{\pm}(p\vec{r}) = \sqrt{\frac{1 + E/c^2}{c^2}} \begin{pmatrix} h_l^{\pm}(pr) \chi_{\Lambda}(\hat{r}) \\ \frac{i p c S_{\kappa}}{E + c^2} h_{\bar{l}}^{\pm}(pr) \chi_{\bar{\Lambda}}(\hat{r}) \end{pmatrix} \quad (20)$$

with the angular momentum  $\bar{l} = l - S_{\kappa}$  for the minor component corresponding to  $-\kappa$  and  $S_{\kappa} = \text{sign}(\kappa)$ . Evaluating all functions in Eqs. (18)–(19) at  $r = r_{cr}$  one finally has

$$t(E) = \frac{i}{2p} [a(E) - b(E)] b^{-1}(E). \quad (21)$$

By a superposition of the wave functions  $\Phi_{\Lambda}$  according to the boundary conditions

$$Z_{\Lambda}(\vec{r}, E) = \sum_{\Lambda'} Z_{\Lambda'\Lambda}(\vec{r}, E) \xrightarrow{r > r_{cr}} \sum_{\Lambda'} j_{\Lambda'}(\vec{r}, E) t(E)_{\Lambda'\Lambda}^{-1} - i p h_{\Lambda}^{+}(\vec{r}, E) \quad (22)$$

one gets an alternative set of linearly independent regular solutions  $Z_{\Lambda}$  to the single-site Dirac equation. These functions are normalized in analogy to nonrelativistic multiple-scattering theory according to the convention of Faulkner and Stocks<sup>33</sup> and allow us straightforwardly to set up the electronic Green's function (see below). The additionally needed irregular solutions  $J_{\Lambda}$  are fixed by the boundary condition

$$J_{\Lambda}(\vec{r}, E) \xrightarrow{r \rightarrow r_{cr}} j_{\Lambda}(\vec{r}, E) \quad (23)$$

and are obtained just by inward integration. The functions  $j_{\Lambda}$  occurring in Eqs. (22) and (23) are the relativistic version of the spherical Bessel functions defined in analogy to Eq. (20) for  $h_{\Lambda}^{\pm}$ .<sup>20</sup>

As an alternative to the direct solution of the above coupled radial differential equations one can also apply the scheme proposed by Dritler<sup>4,34</sup> for the scalar relativistic case. For this purpose the Green's function  $G_{ss}^0$  for the single site system is determined in a first step with the nonspherical potential terms ignored; i.e., by setting  $\bar{V}_L = 0$  and  $B_L = 0$  for  $L \neq (0,0)$ . Here it is advantageous to set up  $G_{ss}^0$  using the regular and irregular solution,  $R^0$  and  $H^0$ , respectively, normalized according to the convention used by the Jülich group (see below). Fixing  $R^0$  and  $H^0$  by the boundary conditions

$$R_{\Lambda}^0(\vec{r}, E) = \sum_{\Lambda'} \begin{pmatrix} g_{\Lambda'\Lambda}^0(r, E) \chi_{\Lambda'}(\hat{r}) \\ if_{\Lambda'\Lambda}^0(r, E) \chi_{\bar{\Lambda}'}(\hat{r}) \end{pmatrix} \\ \xrightarrow{r > r_{cr}} j_{\Lambda}(\vec{r}, E) - ip \sum_{\Lambda'} h_{\Lambda'}^+(\vec{r}, E) t_{\Lambda'\Lambda}(E), \quad (24)$$

$$H_{\Lambda}^0(\vec{r}, E) = \sum_{\Lambda'} \begin{pmatrix} \tilde{g}_{\Lambda'\Lambda}^0(r, E) \chi_{\Lambda'}(\hat{r}) \\ i\tilde{f}_{\Lambda'\Lambda}^0(r, E) \chi_{\bar{\Lambda}'}(\hat{r}) \end{pmatrix} \xrightarrow{r > r_{cr}} h_{\Lambda}^+(\vec{r}, E), \quad (25)$$

with  $t_{\Lambda\Lambda}^0$ , the corresponding single-site  $t$  matrix, the Green's function has the compact form

$$G_{ss}^0(\vec{r}, \vec{r}', E) = -ip \sum_{\Lambda} \{ R_{\Lambda}^0(\vec{r}, E) H_{\Lambda}^{0\times}(\vec{r}', E) \Theta(r' - r) \\ + H_{\Lambda}^0(\vec{r}, E) R_{\Lambda}^{0\times}(\vec{r}', E) \Theta(r - r') \} \quad (26)$$

with

$$R_{\Lambda}^{0\times}(\vec{r}, E) = \sum_{\Lambda'} [g_{\Lambda'\Lambda}^0(r, E) \chi_{\Lambda'}^{\dagger}(\hat{r}); -if_{\Lambda'\Lambda}^0(r, E) \chi_{\bar{\Lambda}'}^{\dagger}] \quad (27)$$

and

$$H_{\Lambda}^{0\times}(\vec{r}, E) = \sum_{\Lambda'} (\tilde{g}_{\Lambda'\Lambda}^0(r, E) \chi_{\Lambda'}^{\dagger}(\hat{r}); -i\tilde{f}_{\Lambda'\Lambda}^0(r, E) \chi_{\bar{\Lambda}'}^{\dagger}). \quad (28)$$

Here and in the following  $\times$  designates the left-hand solutions of the corresponding Dirac-Hamiltonian while  $\dagger$  stands

for the complex transposition operation (see also below). In addition, one should note that in contrast to the scalar relativistic case the wave functions  $R_{\Lambda}^0$  and  $H_{\Lambda}^0$  consist of up to two magnetic partial waves due to the magnetic potential term  $B_L$  for  $L=(0,0)$ . In the next step the solution to the full potential problem is obtained by making use of the Lippmann-Schwinger equation. For the regular and irregular solutions,  $R_{\Lambda}$  and  $H_{\Lambda}$ , respectively, this leads to the following set of coupled radial integral equations:

$$\begin{pmatrix} P_{\Lambda'\Lambda} \\ Q_{\Lambda'\Lambda} \end{pmatrix} = \begin{pmatrix} P_{\Lambda'\Lambda}^0 \\ Q_{\Lambda'\Lambda}^0 \end{pmatrix} + \sum_{\Lambda_{ns}} \left\{ \begin{pmatrix} P_{\Lambda'\Lambda_{ns}}^0 \\ Q_{\Lambda'\Lambda_{ns}}^0 \end{pmatrix} A_{\Lambda_{ns}\Lambda} \right. \\ \left. + \begin{pmatrix} \tilde{P}_{\Lambda'\Lambda_{ns}}^0 \\ \tilde{Q}_{\Lambda'\Lambda_{ns}}^0 \end{pmatrix} B_{\Lambda_{ns}\Lambda} \right\}, \quad (29)$$

$$\begin{pmatrix} \tilde{P}_{\Lambda'\Lambda} \\ \tilde{Q}_{\Lambda'\Lambda} \end{pmatrix} = \begin{pmatrix} \tilde{P}_{\Lambda'\Lambda}^0 \\ \tilde{Q}_{\Lambda'\Lambda}^0 \end{pmatrix} + \sum_{\Lambda_{ns}} \left\{ \begin{pmatrix} P_{\Lambda'\Lambda_{ns}}^0 \\ Q_{\Lambda'\Lambda_{ns}}^0 \end{pmatrix} C_{\Lambda_{ns}\Lambda} \right. \\ \left. + \begin{pmatrix} \tilde{P}_{\Lambda'\Lambda_{ns}}^0 \\ \tilde{Q}_{\Lambda'\Lambda_{ns}}^0 \end{pmatrix} D_{\Lambda_{ns}\Lambda} \right\}. \quad (30)$$

As before [see Eqs. (10)–(13)] we have introduced the auxiliary functions  $P$ ,  $Q$ ,  $P^0$ ,  $Q^0$ ,  $\tilde{P}^0$ , and  $\tilde{Q}^0$ . For the sake of clarity the arguments  $r$  and  $E$  have been suppressed for all functions and the terms connected to the OP potential term in Eq. (6) have been omitted. The  $r$ - and  $E$ -dependent phase functional matrices  $A$ ,  $B$ ,  $C$ , and  $D$  (Ref. 35) occurring in the above equations are given by the following integral equations:

$$A_{\Lambda_{ns}\Lambda}(r) = -ip \int_r^{r_{cr}} dr' \sum_{\Lambda''\Lambda'''} \left\{ \tilde{P}_{\Lambda''\Lambda_{ns}}^0(r') \Delta V_{\Lambda''\Lambda'''}^+(r') P_{\Lambda''\Lambda}(r') + \frac{1}{c^2} \tilde{Q}_{\Lambda''\Lambda_{ns}}^0(r') \Delta V_{\Lambda''\Lambda'''}^-(r') Q_{\Lambda''\Lambda}(r') \right\}, \quad (31)$$

$$B_{\Lambda_{ns}\Lambda}(r) = -ip \int_0^r dr' \sum_{\Lambda''\Lambda'''} \left\{ P_{\Lambda''\Lambda_{ns}}^0(r') \Delta V_{\Lambda''\Lambda'''}^+(r') P_{\Lambda''\Lambda}(r') + \frac{1}{c^2} Q_{\Lambda''\Lambda_{ns}}^0(r') \Delta V_{\Lambda''\Lambda'''}^-(r') Q_{\Lambda''\Lambda}(r') \right\}. \quad (32)$$

$$C_{\Lambda_{ns}\Lambda}(r) = -ip \int_r^{r_{cr}} dr' \sum_{\Lambda''\Lambda'''} \left\{ \tilde{P}_{\Lambda''\Lambda_{ns}}^0(r') \Delta V_{\Lambda''\Lambda'''}^+(r') \tilde{P}_{\Lambda''\Lambda}(r') + \frac{1}{c^2} \tilde{Q}_{\Lambda''\Lambda_{ns}}^0(r') \Delta V_{\Lambda''\Lambda'''}^-(r') \tilde{Q}_{\Lambda''\Lambda}(r') \right\}, \quad (33)$$

$$D_{\Lambda_{ns}\Lambda}(r) = ip \int_r^{r_{cr}} dr' \sum_{\Lambda''\Lambda'''} \left\{ P_{\Lambda''\Lambda_{ns}}^0(r') \Delta V_{\Lambda''\Lambda'''}^+(r') P_{\Lambda''\Lambda}(r') + \frac{1}{c^2} Q_{\Lambda''\Lambda_{ns}}^0(r') \Delta V_{\Lambda''\Lambda'''}^-(r') Q_{\Lambda''\Lambda}(r') \right\}, \quad (34)$$

where again the argument  $E$  has been suppressed. The perturbation term  $\Delta V$  is the nonspherical part of the potential, i.e., without the (0,0) terms in Eqs. (15) and (16), and its matrix elements are defined in analogy to Eq. (14). The

coupled integral equations (29) and (30) can be solved iteratively to the required accuracy by making use of Born's series expansion. As for the scalar relativistic case one gets finally the single-site  $t$  matrix for the full potential case from

$$t_{\Lambda\Lambda'}(E) = t_{\Lambda\Lambda'}^0(E) + \Delta t_{\Lambda\Lambda'}(E), \quad (35)$$

with the correction  $\Delta t_{\Lambda\Lambda'}$  given by<sup>36</sup>

$$-ip\Delta t_{\Lambda\Lambda'}(E) = B_{\Lambda\Lambda'}(r_{cr}, E). \quad (36)$$

### C. Multiple scattering Green's function

The problem of setting up the electronic Green's function  $G(\vec{r}, \vec{r}', E)$  for a solid on the basis of relativistic multiple-scattering theory for arbitrary scalar and vector potentials has been investigated in great detail by Tamura.<sup>9</sup> The corresponding expression for  $G(\vec{r}, \vec{r}', E)$  is given by

$$\begin{aligned} G(\vec{r}, \vec{r}', E) &= \sum_{\Lambda\Lambda'} Z_{\Lambda}^n(\vec{r}, E) \tau_{\Lambda\Lambda'}^{nm}(E) Z_{\Lambda'}^{m\times}(\vec{r}', E) \\ &\quad - \sum_{\Lambda} \{ Z_{\Lambda}^n(\vec{r}, E) J_{\Lambda}^{n\times}(\vec{r}', E) \Theta(r' - r) \\ &\quad + J_{\Lambda}^n(\vec{r}, E) Z_{\Lambda}^{n\times}(\vec{r}', E) \Theta(r - r') \} \delta_{nm} \end{aligned} \quad (37)$$

for  $\vec{r}$  ( $\vec{r}'$ ) within the cell  $n$  ( $m$ ). Here again the normalization in analogy to the nonrelativistic formalism of Faulkner and Stocks<sup>33</sup> for the wave functions  $Z_{\Lambda}$  and  $J_{\Lambda}$  has been used [see Eqs. (22) and (23)]. The reason that we used in contrast to Eq. (37) the Jülich convention for the single-site Green's function  $G_{ss}^0$  in Eq. (26) is that it gets more compact in that way. Using for  $G_{ss}^0$  also the convention Eq. (37) is based on would lead to two sums instead of just one. As a result, Eqs. (29)–(35) would get much more complex and would require more computer time to solve. On the other hand using in Eq. (37) the convention of Faulkner and Stocks; i.e., expressing the Green's function in terms of the scattering path operator  $\tau_{\Lambda\Lambda'}^{ij}$ , does not increase the numerical effort and leads to some advantages when combining the KKR-GF method with the coherent potential approximation (CPA) alloy theory.<sup>37</sup> Of course both conventions are connected to each other just as for the case of spherical potentials [see Eq. (4) in Ref. 38]:

$$\mathbf{G} = (\mathbf{t})^{-1} \boldsymbol{\tau} (\mathbf{t})^{-1} - (\mathbf{t})^{-1}. \quad (38)$$

The boldface notation used indicate here matrices with respect to the site indices and the spin-angular character  $\Lambda$ . The matrix  $\mathbf{G}$  is the structural Green's function matrix used within the Jülich formulation. The most important point to note is that in Eq. (37) the sign  $\times$  indicates that the wave functions  $Z^{\times}$  and  $J^{\times}$  are the left-hand side regular and irregular solutions of the corresponding modified Dirac equation.<sup>9</sup> Fortunately, these are obtained from the same radial differential equations as the conventional right-hand side solutions  $Z_{\Lambda}$  and  $J_{\Lambda}$ ; i.e., from Eqs. (10) and (11) with the potential matrix elements  $V_{\Lambda\Lambda'}^{\pm}$ , replaced by  $V_{\Lambda'\Lambda}^{\pm}$ . For highly symmetric systems one may have the situation that  $V_{\Lambda\Lambda'}^{\pm} = V_{\Lambda'\Lambda}^{\pm}$ . In this case  $Z^{\times}$  and  $J^{\times}$  are obtained from  $Z$  and  $J$  by simple complex conjugation and transposition as indicated in Eqs. (24), (25), (27), and (28) since left- and right-hand side solutions are identical with respect to their radial parts. This applies, in particular, to the single-site problem with spherically symmetric potential terms  $V$  and  $B$ , but also to cubic systems with the magnetization along the  $z$ -

axis, as investigated here. Fortunately, this is still true if the OP term is included in the Dirac equation (1) because here the relation [Eq. (11) in Ref. 9] for the vector potential corresponding to the OP-potential term in Eq. (6) holds.

Finally, the quantity  $\tau_{\Lambda\Lambda'}^{nm}$  in Eq. (37) is the so-called scattering path operator.<sup>33</sup> For an ordered system the site diagonal scattering path operator  $\tau^{nn}$  can be obtained from the BZ integration,

$$\tau_{\Lambda\Lambda'}^{nn} = \frac{1}{\Omega_{BZ}} \int_{\Omega_{BZ}} d^3k [t(E)^{n-1} - G(\vec{k}, E)]_{\Lambda\Lambda'}^{-1}, \quad (39)$$

where  $G(\vec{k}, E)$  is the matrix of the relativistic structure constants.<sup>10</sup>

### D. SCF cycle

With the Green's function  $G(\vec{r}, \vec{r}', E)$  available more or less all quantities of interest can be calculated. In particular, the charge and spin density are obtained via

$$n(\vec{r}) = -\frac{1}{\pi} \text{Im Tr} \int^{E_F} dE G(\vec{r}, \vec{r}, E), \quad (40)$$

$$m(\vec{r}) = -\frac{1}{\pi} \text{Im Tr} \int^{E_F} dE \beta \sigma_z G(\vec{r}, \vec{r}, E). \quad (41)$$

In practice, the energy integration is performed using a contour integration in the complex plane.

Obviously the SCF problem connected with the Dirac equation (1) is just the same as for the nonrelativistic case. In fact the scheme developed by Drittler and co-workers<sup>34,45</sup> to deal with the potential construction and the SCF cycle has been adopted without any changes. In short, this means that the Coulomb part of the potential has been split into an intrasite and intersite part. The former is obtained by straightforward solution of the Poisson equation in real spherical harmonics. The intersite contribution is essentially a Madelung sum of multipole potentials derived from the same representation of the charge distribution on the neighboring sites. In analogy to nonrelativistic spin-density-functional theory the spin-dependent exchange-correlation potentials  $V^{1(1)}$  are obtained from the local charge and spin-magnetization density according to the adopted parametrization. For these an expansion into real spherical harmonics in analogy with Eqs. (15) and (16) is obtained via numerical integration. The corresponding potential terms  $\bar{V}_{xc,L}$  and  $B_L$  are then obtained from

$$\begin{aligned} \bar{V}_{xc,L} &= \frac{1}{2} (V_{xc,L}^{\uparrow} + V_{xc,L}^{\downarrow}), \\ B_{xc,L} &= \frac{1}{2} (V_{xc,L}^{\uparrow} - V_{xc,L}^{\downarrow}). \end{aligned} \quad (42)$$

Finally, in the SCF iterations the Broyden method is used to accelerate the convergence.<sup>39</sup>

At the end of this section it is appropriate to mention some practical aspects. Because close to the nucleus the non-spherical contributions to  $V$  and  $B$  are extremely small, these have been ignored for  $r \leq r_{ns}$ , with  $r_{ns}$  set to 0.2 a.u. (see below). By restricting the angular momentum expansion for the major component of the wave function to  $l_{max}$  one gets a

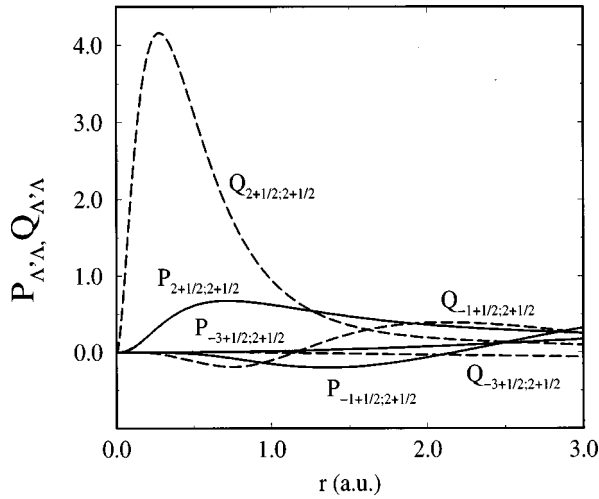


FIG. 1. Radial wave functions  $P_{\Lambda\Lambda'}$  and  $Q_{\Lambda'\Lambda}$  (in atomic units) of the partial waves  $Z_{\Lambda'\Lambda}$  contributing to  $Z_{\Lambda}$  with  $\Lambda = (+2, +1/2)$  for a Fe potential and  $E = 0.6$  Ry. The functions for  $\Lambda' = (-1, +1/2)$  have been scaled up by a factor of  $4 \times 10^3$  for display.

rather natural cutoff for the expansion of all other quantities relevant for the SCF cycle. Because of Eqs. (40) and (41) the expansion for the charge and spin magnetization densities,  $n(\vec{r})$  and  $m(\vec{r})$ , respectively, are restricted to  $2 \times l_{max}$ . Accordingly, the expansion for the potential should also be restricted to  $2 \times l_{max}$ . Finally, the construction of the Coulomb potential, as sketched above, implies that one has to supply the shape functions  $\theta_L(r)$  up to  $4 \times l_{max}$ . Most of these restrictions stem from the triangle condition for the coupling of two angular momenta.

### III. APPLICATION TO bcc Fe, fcc Co, AND fcc Ni

#### A. Calculation of the wave functions

Both schemes presented above to solve the radial Dirac equations (10) and (11) have been implemented. For the direct solution of these equations the Bulirsch-Stoer algorithm<sup>40</sup> has been used. Setting the internal tolerance parameter to  $10^{-6}$  the Wronski relations connecting the various wave functions were fulfilled better than  $10^{-7}$ . An accuracy of  $10^{-10}$  could be achieved by setting the tolerance to  $10^{-10}$ . Using the Born series procedure instead [i.e., Eqs. (29)–(35)] with five iterations led to an accuracy of  $10^{-6}$  for the Wronski relations. However, the computational time for this was about 40% higher than using the Bulirsch-Stoer algorithm with an accuracy of  $10^{-7}$ .

Because the Bulirsch-Stoer algorithm seems to be superior with respect to accuracy and efficiency it has been used throughout for the following applications to the elemental ferromagnets bcc-Fe, fcc-Co, and fcc-Ni.

For all of these calculations the angular momentum expansion for the wave functions has been restricted to  $l_{max} = 2$ . As a consequence of the cubic lattice and the magnetization oriented along the  $z$  axis there are at most three partial waves coupled for  $l_{max} = 2$ . Corresponding results are shown in Fig. 1, where the various wave functions contributing to  $Z_{\Lambda}$  with  $\Lambda = (+2, +1/2)$  are shown for a Fe potential and an energy  $E = 0.6$  Ry. Of course, the diagonal part  $Z_{\Lambda'\Lambda}$  with  $\Lambda' = \Lambda$  dominates, but there are also appreciable contribu-

tions with  $\Lambda' = (-3, +1/2)$  and  $\Lambda' = (-1, +1/2)$  admixed. The former one has  $d$  character as the diagonal partial waves and is primarily due to the magnetic potential term  $B$ . The later contribution with  $s$  character, on the other hand, stems exclusively from the nonspherical potential terms and is about three orders of magnitude smaller than the others.

#### B. Dispersion relation and density of states

Lovatt, Gyroffy, and Guo have calculated the dispersion relation  $E(\vec{k})$  for bcc-Fe using the FP-SPR-KKR together with potentials supplied by self-consistent LAPW calculations.<sup>11</sup> The results for  $E(\vec{k})$  using a self-consistent potential created with the FP-SPR-KKR scheme (see below) is very similar to theirs. In particular, the electronic bands show the same hybridization effect, avoidance of band crossings and anisotropy with respect to the orientation of the magnetization, which is typical of band-structure calculations for spin-polarized systems with the spin-orbit coupling accounted for. All of these mentioned features are found in full accordance with corresponding calculations based on the atomic sphere approximation (ASA) (see, for example, Refs. 36 and 41).

A direct comparison of the dispersion relations calculated using a full and ASA potential, respectively, leads to differences of up to  $10^{-2}$  Ry.<sup>36</sup> Accordingly the corresponding density of states (DOS) curves are found nearly identical for all three systems investigated. Here it seems worth mentioning that for the case of the FP calculations an angular momentum decomposition of the DOS is somewhat ambiguous because of the inclusion of the intersite region.

#### C. Charge and potential distribution

The charge-density distribution for bcc-Fe based on non-selfconsistent FP-SPR-KKR calculations have been given already by Lovatt, Gyroffy, and Guo.<sup>11</sup> Performing such calculations in a self-consistent way does not lead to any qualitative changes. For the nonspherical potential terms  $V_{40}$  and  $B_{40}$  corresponding self-consistent results are shown in Fig. 2. The kinks observed in these curves are connected to those of the shape functions  $\theta_L$ , which possess a kink whenever a cell-centered expanding sphere crosses a plane bounding the Wigner-Seitz cell. Accordingly, the first kink occurs at the muffin-tin radius  $r_{mt}$ , which is the radius of the largest inscribed sphere within the cell.

For comparison the results stemming from scalar relativistic linear augmented plane-wave (LAPW) calculations have been added to Fig. 2. For this purpose the LAPW potential represented in the interstitial region, i.e., for  $r_{mt} \leq r \leq r_{cr}$ , by means of plane waves have been expanded into real spherical harmonics according to Eqs. (15) and (16).

The agreement of both data sets in Fig. 2 is quite satisfying. The differences observed may be ascribed to the mentioned reexpansion of the LAPW potential, the restriction of the angular momentum expansion to  $l_{max} = 2$  for the FP-SPR-KKR calculations, and, last but not least, the inclusion of spin-orbit coupling for the latter. However, a more important consequence of the inclusion of spin-orbit coupling is that the symmetry of the system is reduced compared to the scalar relativistic LAPW calculations. With the mag-

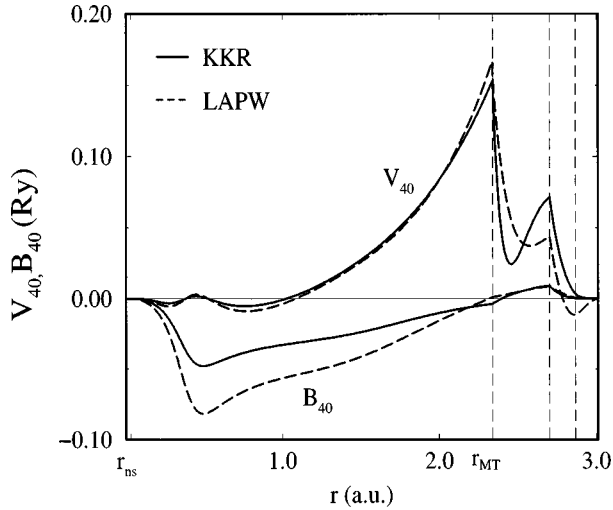


FIG. 2. Nonspherical potential terms  $V_{40}(r)$  and  $B_{40}(r)$  for bcc Fe as obtained from self-consistent FP-SPR-KKR and LAPW calculations.

netization pointing along the  $z$  axis the symmetry is effectively tetragonal.<sup>42</sup> Accordingly, there are now axial contributions to the nonspherical potential as, for example, the terms  $V_{20}$  and  $B_{20}$  shown in Fig. 3. Although these terms are about three orders of magnitude smaller than those shown in Fig. 2 they have nevertheless an important consequence. The Coulomb part  $V_{20}^C$  of  $V_{20}$  at the nuclear site is proportional to the electric-field gradient (EFG) that can be probed for nuclei having a quadrupole moment. As is demonstrated by the results in Fig. 2 accounting for the nonspherical potential only for  $r > r_{ns}$  is well justified. However, on the other hand, this numerical simplification prevents the EFG to be determined directly from the limit  $\lim_{r \rightarrow 0} V_{20}(r)$ . As an alternative the EFG can also be calculated from the corresponding nonspherical charge distribution term  $n_{20}(r)$  within the central Wigner-Seitz cell and a Madelung contribution stemming from the multipoles on the neighboring sites.<sup>43,37</sup>

The results shown above have been obtained ignoring the OP-potential term. This additional term primarily affects the orbital magnetic moment (see below). Its inclusion will

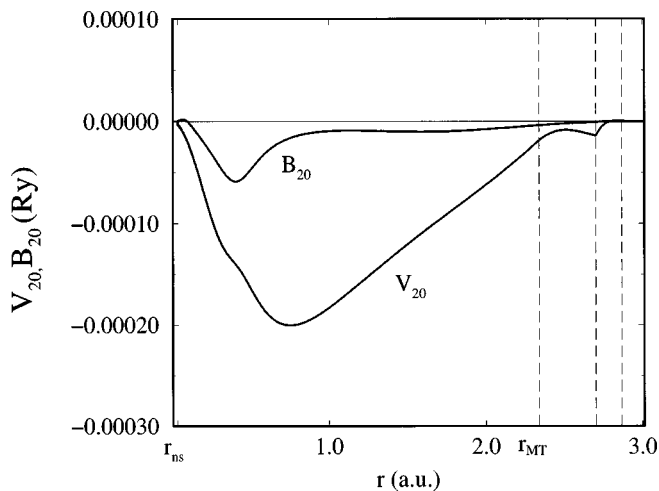


FIG. 3. Nonspherical potential terms  $V_{20}(r)$  and  $B_{20}(r)$  for bcc Fe as obtained from self-consistent FP-SPR-KKR calculations.

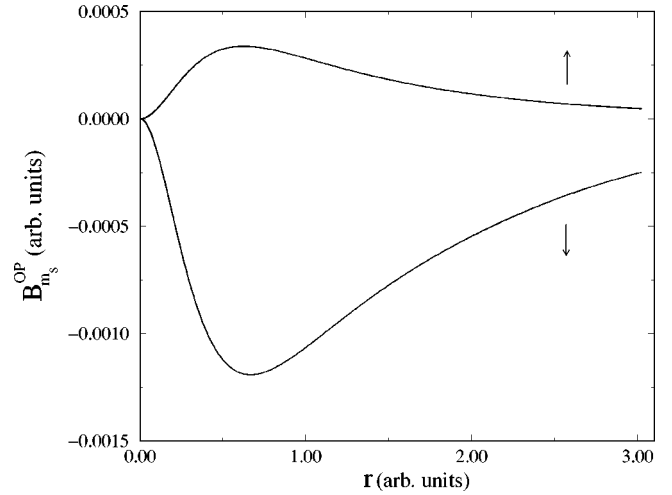


FIG. 4. The OP potential term  $B_{m_s}^{OP}$  for bcc Fe as calculated by the self-consistent FP-OP-SPR-KKR.

therefore hardly affect the scalar potentials  $V$  and  $B$ . For bcc-Fe, the spin-resolved OP-potential terms  $B_{m_s}^{OP}$  obtained from a self-consistent calculation are shown in Fig. 4. As one notes, both curves are very similar. Their simple radial dependence of course stems from their connection with the radial charge distribution for the  $d$  electrons [see Eq. (5)]. Their sign and magnitude, on the other hand, is primarily determined by the expectation value  $\langle l_z \rangle_{d, m_s}$ . This quantity obviously has different signs for the majority and minority spin systems and is bigger in magnitude for the latter (see also below). The most important point to note with respect to the curves in Fig. 4 is that the radial variation of the orbital polarization-vector potential is extremely different from that occurring within a CDFT calculation.<sup>27</sup> This is of course not surprising because the physical mechanism behind both schemes is quite different.

#### D. Orbital current-density distribution

An important consequence of the inclusion of spin-orbit coupling within a band-structure calculation for a spin-polarized solid is that its orbital angular momentum is no more quenched. This corresponds to the occurrence of a finite paramagnetic orbital current density  $\vec{j}_p$  (the adjective paramagnetic will be omitted in the following because external magnetic fields were assumed to be absent; i.e., the physical and paramagnetic current densities are identical).

Together with the spin-resolved particle density  $n_\sigma$  this quantity supplies the basic variable within CDFT as formulated by Vignale and Rasolt.<sup>24</sup> Although this scheme has not been used here (for a recent application of CDFT to magnetic solids see Ref. 27) the current density  $\vec{j}_p$  has been calculated in a spin-resolved way, because it enters in this form the so-called Vignale-Rasolt equations of CDFT, which replace the Kohn-Sham equations of SDFT. This means that  $\vec{j}_{p, \sigma}$  has been obtained from

$$\vec{j}_{p, \sigma} = -\frac{1}{\pi} \text{Im Tr} \int^{E_F} dE \frac{1}{i} [\vec{\nabla} - \vec{\nabla}'] P_\sigma G(\vec{r}, \vec{r}', E) |_{\vec{r}=\vec{r}'}, \quad (43)$$

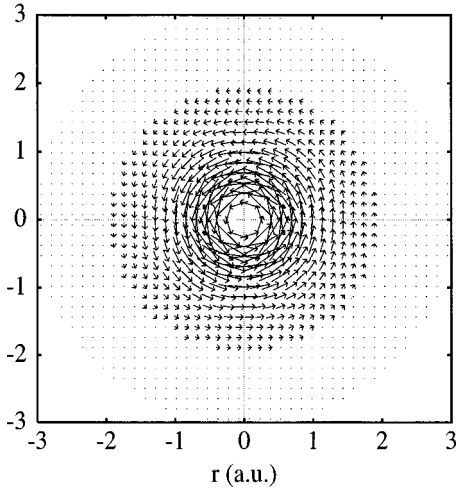


FIG. 5. Orbital current density  $\vec{j}_p$  for bcc Fe in the (001)-plane (in arbitrary units). For display  $\vec{j}_p$  has been weighted with  $r^2$ .

with the spin projection operator  $P_\sigma = \frac{1}{2}(1 \pm \beta\sigma_z)$ .

Results obtained that way for the spin-integrated orbital current density  $\vec{j}_p = \sum_\sigma \vec{j}_p$  of bcc Fe are shown in Fig. 5. Here the direction and magnitude of  $\vec{j}_p$  is represented by arrows for the (001) plane with the  $z$  and magnetization axes pointing upwards. At first sight the current-density distribution seems to be rotational symmetric. However, a closer look reveals that it has in fact a lower symmetry. This is demonstrated in Fig. 6, which gives the radial component of  $\vec{j}_p$  within the (001) plane (this component is about 2–3 orders of magnitude smaller than  $\vec{j}_p$  itself and has been scaled by a factor of approximately 350 with respect to Fig. 5). As one notes, there is only a fourfold symmetry axis along the  $z$  axis. For the paramagnetic state the  $x$  and  $y$  axes as well as the diagonal axes in between would be twofold symmetry axes. Obviously, the corresponding symmetry operation  $C_2$  is missing here because of the ferromagnetic state and the spin-orbit coupling accounted for. However, one can also clearly see from Figs. 5 and 6 that this symmetry operations com-

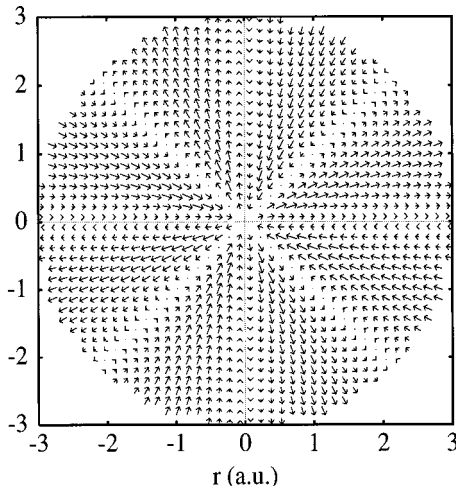


FIG. 6. Radial component of the orbital current density  $\vec{j}_p$  for bcc Fe in the (001) plane (in arbitrary units). For display  $\vec{j}_p$  has been weighted with  $r^2$ .

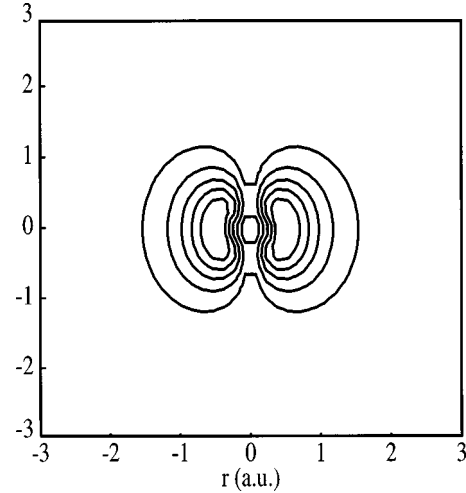


FIG. 7. Magnitude of  $r^2 \vec{j}_p$  for bcc Fe in the (100) plane (in arbitrary units). Starting from one of the innermost kidney-shaped isolines  $|r^2 \vec{j}_p|$  decreases monotonously in constant steps when going outwards from one isoline to the adjacent one.

pared with the time inversion  $T$  result in true symmetry operations ( $TC_{2\perp}$ ) for the ferromagnetic state.<sup>42</sup>

The distribution of the current density  $\vec{j}_p$  within the (100) plane, which includes the magnetization axis, is shown in Fig. 7, where the magnitude of  $r^2 \vec{j}_p$  is represented by means of iso-intensity lines. As could already be seen in Fig. 5 the current is strongly concentrated in the inner region of the atom for any direction in space. In addition, one notes that the current density weighted with  $r^2$  takes its maximum on the (001) plane at about  $0.5a_0$  distance from the nucleus. This is demonstrated once more in Fig. 8 where the magnitude of  $r^2 \vec{j}_p$  averaged with respect to  $\phi$  within the (001)

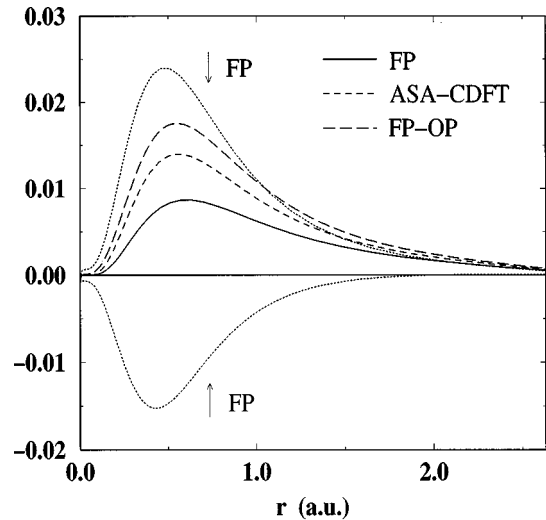


FIG. 8. Magnitude of  $r^2 \vec{j}_p$  for bcc Fe in the (100) plane and averaged with respect to its  $\phi$  dependence. The various curves show results stemming from FP-SPR-KKR (FP) calculations based on the plain SDFT-Dirac equation (1), calculations including the OP term (FP-OP) and work done within CDFT using the ASA-SPR-KKR (ASA-CDFT) (Ref. 27). In addition the decomposition of the FP result into its spin-projected contributions  $\vec{j}_p^{(\uparrow)}$  is given marked by  $\uparrow$ FP,  $\downarrow$ FP.

TABLE I. Spin- and orbital-magnetic moments,  $\mu_{spin}$  and  $\mu_{orb}$ , respectively, for bcc Fe, fcc Co, and fcc Ni using the various calculation schemes mentioned in the text. The experimental values have been taken from Refs. 47 and 48.

	Fe		Co		Ni	
	$\mu_{spin}$	$\mu_{orb}$	$\mu_{spin}$	$\mu_{orb}$	$\mu_{spin}$	$\mu_{orb}$
FP	2.240	0.050	1.585	0.073	0.565	0.046
ASA	2.282	0.054	1.580	0.075	0.579	0.047
FP-OP	2.240	0.080	1.585	0.113	0.566	0.062
ASA-OP	2.284	0.085	1.580	0.117	0.582	0.057
Expt.	2.13	0.08	1.52	0.14	0.57	0.05

plane is shown. The decrease of the current density for  $r \geq 1a_0$  is roughly proportional to  $r^{-3}$ . This is in line with the crude estimation  $\vec{j}_p(r) \approx [n(\vec{r})]/r$ , which is based on the fact that  $\vec{j}_p$  is by far dominated by its  $\phi$  component.

As one can already guess from the radial wave functions shown in Fig. 1,  $\vec{j}_p$  is primarily connected to the  $d$  electrons. This expectation is confirmed by a detailed angular momentum analysis that shows that  $\vec{j}_p$  is indeed by far dominated by its  $d$ -electron contribution. Calculating the current density  $\vec{j}_p$  in a spin-projected way, one finds that there is also a small contribution to  $j_p^{\uparrow(\downarrow)}$  arising from  $s$ -like wave functions leading to a small plateau for the corresponding curves in Fig. 8. These contributions are a pure relativistic effect because they stem from the minor component of the  $s$ -like wave functions having  $p$  character. Summing both spin contributions to  $\vec{j}_p$  one can see from Fig. 8 that these contributions cancel each other to a large extent. The spin decomposition of  $\vec{j}_p$  also demonstrates that the orbital current for Fe stems primarily from the minority spin system. This imbalance of the two spin subsystems even increases when going from Fe to Co and Ni, because the majority subband gets more and more filled. Because there is a direct relationship between the orbital current and the orbital magnetic moment  $\mu_{orb}$  (see below) it is obvious that  $\mu_{orb}$  is also dominated by the minority spin contribution. This has also been found before by Eriksson *et al.*,<sup>44</sup> who used the LMTO-ASA with the spin-orbit coupling accounted for in a variational step.

In Fig. 8 the results of FP calculations for  $\vec{j}_p$  including the OP term (FP-OP) have been added. As one can see, the variation of the corresponding curve with the distance  $r$  from the nucleus is just the same as for the calculation based on the plain Dirac equation (1). This also holds for results obtained using the SPR-KKR within current-density-functional theory and using the ASA.<sup>27</sup> This implies that the radial dependence of the vector potential included in the Dirac equation does not have much influence on that of the orbital current. Its absolute magnitude, however, is quite different for the three sets of calculations. According to this one gets for the plain FP, the FP-OP, and the ASA-CDFT calculation an orbital magnetic moment of 0.05, 0.08, and  $0.07\mu_B$ , respectively (see Table I and Ref. 27).

### E. Magnetic moments and hyperfine fields

For the calculation of the spin and orbital magnetic moments,  $\mu_{spin}$  and  $\mu_{orb}$ , respectively, the conventional expressions<sup>22</sup>

$$\mu_{spin} = -\frac{\mu_B}{\pi} \text{Im Tr} \int^{E_F} dE \int d^3r \beta \sigma_z G(\vec{r}, \vec{r}, E) \quad (44)$$

and

$$\mu_{orb} = -\frac{\mu_B}{\pi} \text{Im Tr} \int^{E_F} dE \int d^3r \beta l_z G(\vec{r}, \vec{r}, E) \quad (45)$$

have been used. Of course,  $\mu_{spin}$  is nothing but the spin magnetization density integrated over the Wigner-Seitz cell. The connection of  $\mu_{orb}$  and the orbital current density  $\vec{j}_p$  discussed above is less straightforward. According to the Gordon decomposition of the total electronic current,  $\vec{j}_p$  is connected with the orbital angular momentum  $\vec{l}$  via the equation

$$\vec{j}_p = \sqrt{2} \beta \vec{\nabla} \times \vec{l}, \quad (46)$$

where external magnetic fields have been assumed to be absent. For a rotational symmetric current distribution with  $\vec{j}_{p,\phi}$  as the only nonvanishing component of  $\vec{j}_p$  this implies the simple relationship

$$\langle \beta l_z(\vec{r}) \rangle = \frac{1}{2\sqrt{2}} \langle r \vec{j}_{p,\phi}(\theta, r) \rangle. \quad (47)$$

The results for the orbital current shown for bcc-Fe in Fig. 8 are quite typical for the late  $3d$  elements. This means that the minority spin contribution exceeds that of the majority spin system throughout the Wigner-Seitz cell leading altogether to a positive orbital magnetic moment, i.e., an orbital moment aligned parallel to the spin moment. As can be seen from Table I, this applies to all three metals and the various schemes applied. The corresponding calculations have been performed in all cases using an angular momentum expansion up to  $l_{max}=2$ .

Table I shows that the difference between the FP and ASA calculations are quite small. For  $\mu_{spin}$  the difference is at most 2%, while for  $\mu_{orb}$  it reaches about 9%. As found before for SPR-KKR calculations using the ASA, one notes that also for the FP case the inclusion of the OP-potential term has only a minor influence on  $\mu_{spin}$ . For  $\mu_{orb}$ , on the other hand, inclusion of this correction term is essential to achieve good agreement with experiment. As found also by Trygg *et al.*,<sup>45</sup> who performed FP-LMTO calculations with the spin-orbit coupling included in the variational step, it is found that there is no conflict between the FP mode and using the OP term, which was expected sometimes. From Table I one can clearly see that the OP term leads for the ASA as well as for the FP calculations to nearly the same enhancement of the orbital moments.

The magnetization density of a magnetically ordered solid gives rise to a magnetic hyperfine field  $B_{hf}$  at the sites of the nuclei. The most natural way to calculate this field is supplied by Breit's hyperfine interaction Hamiltonian, which gives the nuclear Zeeman energy caused by the total electronic current-density distribution. Within the Green's-function formalism used here, this implies for the hyperfine field the expression

TABLE II. Hyperfine fields  $B_{hf}$  for bcc Fe, fcc Co, and fcc Ni using the ASA- and FP-SPR-KKR. In both cases a decomposition into core and valence-band contribution is given, with the latter split into its  $s$ ,  $p$ , and  $d$  parts. The experimental data have been taken from Refs. 47 and 48.

	Fe			Co			Ni		
	FP	ASA	Expt.	FP	ASA	Expt.	FP	ASA	Expt.
$s$	-33.2	-37.8		-48.1	-55.2		-18.4	-16.0	
$p$	0.8	0.7		1.6	1.7		0.8	0.9	
$d$	19.2	21.0		43.9	45.0		37.0	37.4	
Val.	-13.2	-16.0		-2.7	-8.6		19.5	22.3	
Core	-252.5	-248.7		-185.6	-180.9		-69.6	-69.6	
Tot.	-265.7	-264.7	-339	-188.3	-189.5	-215	-50.1	-47.3	-75

$$B_{hf} = -\frac{1}{\mu_n \pi} \text{Im Tr} \int^{E_F} dE \int d^3r e \vec{\alpha} \cdot \left( \vec{\mu}_n \times \frac{\vec{r}}{r^3} \right) G(\vec{r}, \vec{r}, E), \quad (48)$$

where  $\mu_n$  is the nuclear magnetic moment. Corresponding results for bcc Fe, fcc Co, and fcc Ni are summarized in Table II for calculations based on the FP and the ASA mode. Here the fields have been split into their core and valence electron contributions. In addition, the latter are decomposed with respect to the angular momentum. For the various contributions one finds changes up to around 10% when going from the ASA to the FP mode. However, for the total fields these changes nearly cancel each other leading to rather small differences between the ASA and FP result. Accordingly, the discrepancy of the theoretical and experimental hyperfine fields for the pure  $3d$  elements Fe, Co, and Ni is not removed by performing the calculations in a FP mode. Here it seems to be appropriate to emphasize that the contribution of the  $p$ - and  $d$ -valence electrons to  $B_{hf}$  are of relativistic origin; i.e., these spin-orbit-induced contributions cannot be accounted for within a nonrelativistic or scalar relativistic calculation. Although the  $p$ - and  $d$ -hyperfine fields could also come from the nuclear spin-electron spin interaction, an analysis clearly shows that it stems nearly exclusively from a coupling of the nuclear spin to the electronic orbital magnetic moment.<sup>46</sup> Alternatively, and in line with Breit's formula, one can say that these contributions to  $B_{hf}$  are a direct consequence of the orbital current density  $\vec{J}_p$ .

### F. Lattice properties

The theoretical equilibrium lattice constants  $a_{eq}$  of bcc Fe, fcc Co, and fcc Ni have been determined on the basis of

TABLE III. Equilibrium lattice constants (in a.u.) for bcc Fe and fcc Ni from various calculations as well as experiment.

	bcc-Fe	fcc-Ni
ASA-LMTO (Ref. 49)	5.44	
FP-LAPW (Ref. 50)	5.22	
KKR (Ref. 19)	5.27	6.55
FP-KKR (Ref. 51)	5.205	
FP-SPR-KKR	5.332	6.636
Experiment	5.406	6.658

total energy ( $E_{tot}$ ) calculations performed using the FP-SPR-KKR. For this purpose the conventional expression

$$E_{tot} = \sum_{i=1}^N \epsilon_i - \int d^3r [V(\vec{r})n(\vec{r}) + B(\vec{r})m(\vec{r})] + \int d^3r \int d^3r' \frac{n(\vec{r})n(\vec{r}')}{|\vec{r} - \vec{r}'|} + E_{xc}[n, m] \quad (49)$$

has been used.

To determine the equilibrium lattice constant  $a_{eq}$  we fit the total energy  $E_{tot}(V)$ , calculated for several volumes  $V$ , to an analytic formula

$$E(V) = \sum_{n=1}^4 b_n V^{-(2/3)(n-2)} \quad (50)$$

and determine  $a_{eq}$  by minimizing the  $E_{tot}(V)$  of Eq. (50). The results are given in Table III together with some other theoretical as well as experimental data. Obviously there is quite good agreement among the various theoretical lattice parameters and also with experiment. Nevertheless it should be noted that the difference between the FP-KKR and the FP-SPR-KKR data is not only due to the inclusion of relativistic effects in the latter case but also due to the different angular momentum expansion used.

Concerning the bulk modulus the situation is less favorable as for the equilibrium lattice constant (see Table IV). Here, one finds as for all other previous calculations values that are by around 60% too small compared to experiment. This is a typical error of the LDA approximation, leading to an overbinding of the system with a too large cohesion energy, a slightly too small lattice constant, and a too large bulk modulus. This discrepancy could be removed by using a gradient corrected exchange-correlation potential. Without

TABLE IV. Bulk modulus (in  $10^9$  Pa) for bcc Fe and fcc Ni from various calculations as well as experiment.

	bcc-Fe	fcc-Ni
ASA-LMTO (Ref. 49)	170	
FP-LAPW (Ref. 50)	251	
KKR (Ref. 19)	220	230
FP-SPR-KKR	220	222
Experiment	172	186

doubt, this would also happen for the FP-SPR-KKR calculations. However, it is a now common experience that the available gradient-corrected parametrizations are not suitable for heavy elements for which relativistic effects are more pronounced than for the systems studied here. For that reason these corrections have not been included in the developed program package so far.

#### IV. SUMMARY

The theoretical basis of the FP-SPR-KKR method has been sketched and the most important details of a corresponding implementation have been discussed. A number of results have been presented, that were primarily meant to illustrate the consequences for the electronic properties of a spin-polarized system if in addition to relativistic effects also the nonspherical shape and eventually also the orbital polar-

ization mechanism are accounted for. For the magnetic moments and hyperfine fields of bcc Fe, fcc Co, and fcc Ni the impact of the FP-mode was found to be relatively small. Nevertheless, these applications revealed several details of the electronic structure and demonstrated the feasibility of self-consistent FP-SPR-KKR calculations. In fact, corresponding calculations have been done now for disordered alloys using the CPA.<sup>37</sup>

#### ACKNOWLEDGMENTS

Support of this work by the Deutsche Forschungsgemeinschaft within the Schwerpunkt Theorie relativistischer Effekte in der Chemie und Physik schwerer Elemente is also gratefully acknowledged. The paper has profited from collaborations within the TMR network "Interphase Magnetism" of the European Union.

- 
- <sup>1</sup>J. Koringa, *Physica* (Amsterdam) **XIII**, 392 (1947).  
<sup>2</sup>W. Kohn and N. Rostoker, *Phys. Rev.* **94**, 1111 (1953).  
<sup>3</sup>H. Bross and K. H. Anthony, *Phys. Status Solidi* **22**, 667 (1967).  
<sup>4</sup>B. Drittler, M. Weinert, R. Zeller, and P. H. Dederichs, *Solid State Commun.* **79**, 31 (1991).  
<sup>5</sup>B. Drittler, M. Weinert, R. Zeller, and P. H. Dederichs, in *Application of Multiple Scattering Theory to Materials Science*, edited by W. H. Butler, P. H. Dederichs, A. Gonis, and R. Weaver, MRS Symposia Proceedings No. 253 (Materials Research Society, Pittsburgh, 1992), p. 185.  
<sup>6</sup>P. H. Dederichs, B. Drittler, and R. Zeller, in *Application of Multiple Scattering Theory to Materials Science* (Ref. 5), p. 185.  
<sup>7</sup>N. Papanikolaou, R. Zeller, P. H. Dederichs, and N. Stefanou, *Phys. Rev. B* **55**, 4157 (1997).  
<sup>8</sup>N. Papanikolaou, R. Zeller, P. H. Dederichs, and N. Stefanou, *Comput. Mater. Sci.* **8**, 131 (1997).  
<sup>9</sup>E. Tamura, *Phys. Rev. B* **45**, 3271 (1992).  
<sup>10</sup>X. Wang *et al.*, *Phys. Rev. B* **46**, 9352 (1993).  
<sup>11</sup>S. C. Lovatt, B. L. Gyorffy, and G.-Y. Guo, *J. Phys.: Condens. Matter* **5**, 8005 (1993).  
<sup>12</sup>S. B. der Kellen and A. J. Freeman, *Phys. Rev. B* **54**, 11 187 (1996).  
<sup>13</sup>M. Fluchtmann, M. Grass, J. Braun, and G. Borstel, *Phys. Rev. B* **52**, 9564 (1995).  
<sup>14</sup>J. W. Krewer and R. Feder, *Physica B* **172**, 135 (1991).  
<sup>15</sup>M. S. S. Brooks, *Physica B* **130**, 6 (1985).  
<sup>16</sup>H. Ebert and M. Battocletti, *Solid State Commun.* **98**, 785 (1996).  
<sup>17</sup>A. H. MacDonald and S. H. Vosko, *J. Phys. C* **12**, 2977 (1979).  
<sup>18</sup>M. V. Ramana and A. K. Rajagopal, *J. Phys. C* **12**, L845 (1979).  
<sup>19</sup>V. L. Moruzzi, J. F. Janak, and A. R. Williams, *Calculated Electronic Properties of Metals* (Pergamon, New York, 1978).  
<sup>20</sup>M. E. Rose, *Relativistic Electron Theory* (Wiley, New York, 1961).  
<sup>21</sup>A. P. Cracknell, *J. Phys. C* **2**, 1425 (1969).  
<sup>22</sup>H. Ebert, P. Strange, and B. L. Gyorffy, *J. Phys. F* **18**, L135 (1988).  
<sup>23</sup>O. Eriksson, B. Johansson, and M. S. S. Brooks, *J. Phys.: Condens. Matter* **1**, 4005 (1989).  
<sup>24</sup>G. Vignale and M. Rasolt, *Phys. Rev. Lett.* **59**, 2360 (1987).  
<sup>25</sup>G. Vignale and M. Rasolt, *Phys. Rev. Lett.* **62**, 115 (1989).  
<sup>26</sup>G. Vignale, in *Current Density Functional Theory and Orbital Magnetism*, Vol. 337 of *Nato Advanced Study Institute Series, Series B: Physics*, edited by E. K. U. Gross and R. M. Dreizler (Plenum Press, New York, 1995), p. 485.  
<sup>27</sup>H. Ebert, M. Battocletti, and E. K. U. Gross, *Europhys. Lett.* **40**, 545 (1997).  
<sup>28</sup>S. Doniach and C. Sommers, in *Valence Fluctuations in Solids*, edited by L. M. Falicov, W. Hanke, and M. B. Maple (North-Holland, Amsterdam, 1981), p. 349.  
<sup>29</sup>R. Feder, F. Rosicky, and B. Ackermann, *Z. Phys. B* **52**, 31 (1983).  
<sup>30</sup>P. Strange, J. B. Staunton, and B. L. Gyorffy, *J. Phys. C* **17**, 3355 (1984).  
<sup>31</sup>B. Ackermann, Ph.D. thesis, University of Duisburg, 1985.  
<sup>32</sup>H. Ebert and B. L. Gyorffy, *J. Phys. F* **18**, 451 (1988).  
<sup>33</sup>J. S. Faulkner and G. M. Stocks, *Phys. Rev. B* **21**, 3222 (1980).  
<sup>34</sup>B. Drittler, Ph.D. thesis, RWTH Aachen, 1990.  
<sup>35</sup>F. Calogero, *Variable Phase Approach to Potential Scattering* (Academic Press, New York, 1967).  
<sup>36</sup>T. Huhne, Master's thesis, University of Munich, 1997.  
<sup>37</sup>C. Zecha, Master's thesis, University of Munich, 1997.  
<sup>38</sup>R. Zeller *et al.*, *Phys. Rev. B* **52**, 8807 (1995).  
<sup>39</sup>S. Blügel, Ph.D. thesis, RWTH Aachen, 1987.  
<sup>40</sup>W. H. Press, B. P. Flannery, S. A. Teukolsky, and W. T. Vetterling, *The Art of Scientific Computing* (Cambridge University Press, London, 1986).  
<sup>41</sup>P. Strange, H. Ebert, J. B. Staunton, and B. L. Gyorffy, *J. Phys.: Condens. Matter* **1**, 2959 (1989).  
<sup>42</sup>A. P. Cracknell, *Phys. Rev. B* **1**, 1261 (1970).  
<sup>43</sup>B. Drittler, M. Weinert, R. Zeller, and P. H. Dederichs, *Phys. Rev. B* **42**, 9336 (1990).  
<sup>44</sup>O. Eriksson *et al.*, *Phys. Rev. B* **41**, 11 807 (1990).  
<sup>45</sup>J. Trygg, B. Johansson, O. Eriksson, and J. M. Wills, *Phys. Rev. Lett.* **75**, 2871 (1995).  
<sup>46</sup>M. Battocletti, Ph.D. thesis, University of München, 1997.  
<sup>47</sup>M. B. Stearns, in *Magnetic Properties of 3d, 4d and 5d Elements, Alloys and Compounds*, edited by K.-H. Hellwege and O. Made-

- lung, Landolt-Börnstein, New Series, Group III, Vol. 19, Pt. a (Springer, Berlin, 1987).
- <sup>48</sup>D. Bonnenberg, K. A. Hempel, and H. P. Wijn, in *Title*, edited by K.-H. Hellwege and O. Madelung, Landolt-Börnstein, New Series, Group III, Vol. 19, Pt. a (Springer, Berlin, 1987).
- <sup>49</sup>P. Bagno, O. Jepsen, and O. Gunnarsson, Phys. Rev. B **40**, 1997 (1989).
- <sup>50</sup>D. J. Singh, W. E. Pickett, and H. Krakauer, Phys. Rev. B **43**, 11 628 (1991).
- <sup>51</sup>B. Nonas, Master's thesis, RWTH Aachen, 1996.